The Canadian Mineralogist
Vol. 44, pp. 415-431 (2006)

DISSOLUTION OF URANYL-OXIDE-HYDROXY-HYDRATE MINERALS. I. CURITE

MICHAEL SCHINDLER[§]

Department of Geological Sciences, University of Manitoba, Winnipeg, Manitoba R3T 2N2, Canada

PETRE MANDALIEV[¶]

Institut für Mineralogie, Universität Münster, D–48149 Münster, Germany

FRANK C. HAWTHORNE

Department of Geological Sciences, University of Manitoba, Winnipeg, Manitoba R3T 2N2, Canada

ANDREW PUTNIS

Institut für Mineralogie, Universität Münster, D–48149 Münster, Germany

ABSTRACT

Dissolution experiments on synthetic crystals of curite, $Pb^{2+}{}_3(H_2O)_2[(UO_2)_4O_4(OH)_3]_2$, were done in HCl–$H_2O$ solutions of pH 2.1 and 3.5, in doubly distilled water, in Sr^{2+}–HCl–H_2O solutions of pH 2.7 and 5.5, and in Na_2CO_3 solutions of pH 10.5 for 24 h at 60°C. Examination by atomic force microscopy and optical microscopy reveals the formation of etch pits under near-neutral to strongly acidic solutions, and the formation of hillocks under strongly basic solutions. A new approach to the morphology of uranyl-oxide minerals is used to calculate the stability of edges and the morphology of etch pits and hillocks formed on the basal surface of curite. These calculations predict that the probability of occurrence of edges decreases in the sequence: [001], [011], [0*kl*], $k < l$, [0*kl*], $k > l$, [010]. Edges along the basal surface and of all observed etch-pits and hillocks are [001], [110] and [0*kl*], $k < l$, in agreement with the predictions. Etch pits formed at lower pH have lower relief and larger lateral extent than etch pits formed at higher pH, in accord with a decrease in stability of the edges with decreasing pH. Etch pits on the same basal surface have identical orientations, which violates the presence of a two-fold screw axis in the symmetry of the bulk structure. Cross sections of etch pits are characterized by steep edges and convex surfaces. A growth model of an etch pit formed in doubly distilled water explains this morphology by different rates of dissolution perpendicular to edges defined by right and left terminations of polyhedron chains. Differences in the symmetry of etch pits formed in Sr^{2+}-bearing and non-Sr^{2+}-bearing solutions are attributed to a nonstoichiometric detachment of polyhedra in the absence of Sr^{2+} in the vicinity of the etch pits. The formation of hillocks under basic conditions and an increase in the density of etch pits with decreasing pH suggest that the formation of etch pits depends more on the degree of protonation of the basal face and its edges than on the degree of undersaturation of the solution with respect to curite.

Keywords: curite, uranium, dissolution, atomic force microsopy, bond valence, radionuclide, adsorption.

SOMMAIRE

Nos expériences de dissolution ont porté sur des cristaux synthétiques de curite, $Pb^{2+}{}_3(H_2O)_2[(UO_2)_4O_4(OH)_3]_2$, en contact avec des solutions HCl–H_2O d'un pH de 2.1 et 3.5, de l'eau doublement distillée, des solutions de Sr^{2+}–HCl–H_2O à un pH de 2.7 et 5.5, et des solutions de Na_2CO_3 d'un pH de 10.5 pour 24 heures à 60°C. Un examen par microscopie à force atomique et par microscopie optique révèle la formation de figures de corrosion en présence de solutions variant de presque neutres à fortement acides, et la formation de monticules de croissance où les solutions sont fortement basiques. Une nouvelle approche à la morphologie des minéraux d'oxydes uranylés a été utilisée pour calculer la stabilité des arêtes et la morphologie des figures de corrosion et des monticules de croissance formés sur la surface de base de la curite. Ces calculs prédisent que la probabilité de former des arêtes diminue selon la séquence: [001], [011], [0*kl*], $k < l$, [0*kl*], $k > l$, [010]. Les arêtes le long de la surface de base et de toutes les figures de corrosion et les monticules de croissance observés sont [001], [110] et [0*kl*], $k < l$, ce qui concorde avec les prédictions. Les figures de corrosion formées à plus faible pH possèdent un relief plus faible et une étendue latérale plus

§ *E-mail address*: schindl0@cc.umanitoba.ca
¶ *Present address*: Laboratory for Waste Management, Paul Scherrer Institute, OHLD 111, CH–5232 Villigen PSI, Switzerland.

grande que celles formées à pH plus élevé, en accord avec une diminution de la stabilité des arêtes à mesure que diminue le pH. Les figures de corrosion sur une même surface de base font preuve d'orientations identiques, en violation avec la présence d'un axe hélical d'ordre deux comme élément de symétrie de la structure globale. Des coupes transversales des figures de corrosion seraient caractérisées par des arêtes raides et des surfaces convexes. Un modèle de croissance d'une figure de corrosion formée dans l'eau doublement distillée explique cette morphologie en invoquant des taux différentiels de dissolution perpendiculairement aux arêtes définies par les terminaisons droites et gauches des chaînes de polyèdres. Des différences dans la symétrie des figures de corrosion formées dans un milieu contenant le Sr^{2+} ou bien en l'absence de solutions contenant le Sr^{2+} seraient attribuables à un détachement nonstoichiométrique de polyèdres en l'absence de Sr^{2+} près des figures de corrosion. D'après la formation de monticules de croissance et une augmentation de la densité des figures de corrosion avec une diminution du pH, la formation des figures de corrosion dépendrait davantage du degré de protonation de la surface de base et ses arêtes que du degré de sous-saturation de la solution par rapport à la curite.

(Traduit par la Rédaction)

Mots-clés: curite, uranium, dissolution, microsopie à force atomique, valence de liaison, radionucléide, adsorption.

Introduction

Uranyl oxide minerals are common constituents of the weathered zones in uranium mine and mill tailings (Abdelouas *et al*. 1999). They form in soils contaminated with actinides (Buck *et al*. 1996) and are likely to be common products of spent nuclear fuel in a geological repository such as the proposed Yucca Mountain repository in Nevada (Finn *et al*. 1996, Wronkiewicz *et al*. 1996). Despite their environmental importance, our understanding of water – mineral – surface interactions such as crystal growth, dissolution and adsorption lags behind that for other mineral groups, owing primarily to the structural complexity of uranyl oxide minerals and experimental difficulties associated with small crystals of poor quality.

In this paper, we examine dissolution processes that affect the basal surface of the common uranyl-hydroxy-hydrate mineral curite, $Pb^{2+}{}_3(H_2O)_2[(UO_2)_4O_4(OH)_3]_2$ as a function of pH and the presence of Sr cations in solution, and compare the observed etch-pit morphology with the predicted morphology calculated with the approach of Schindler *et al*. (2004a, b).

Background Information

Pb^{2+}-uranyl-hydroxy-hydrate minerals generally have a lower solubility than other uranyl-hydroxy-hydrate minerals (Finch & Murakami 1999). Hence, dissolution experiments must be done either over a longer period of time or at elevated temperatures and pressures. Recently, dissolution processes for low-solubility minerals have been examined *in situ* with a hydrothermal Atomic Force Microscope (HAFM, Higgins *et al*. 1998). Here, the kinetics of etch-pit formation, step retreat and formation of hillocks was observed from 20 to 130°C and from 1 to 35 bar (*e.g.,* Aldushin *et al*. 2004a, b, Jordan *et al*. 2001). However, we focus here on the change in stability of edges and faces with pH, and on the presence of cations in solution (rather than on the kinetics of the corresponding surface-processes). For this purpose, suitable information can be collected from batch-dissolution experiments and subsequent examination of the basal face of curite with a conventional AFM.

Dissolution experiments in the presence of Sr^{2+} are of considerable interest because ^{90}Sr radionuclides are products of the radioactive decay of spent nuclear fuel (Finn *et al*. 1996). Radionuclides will be immobilized either through incorporation into the structure of alteration phases (Burns *et al*. 1997, 2004, Chen *et al*. 1999, 2000) or through adsorption onto their surface. Burns & Hill (2000) and Burns & Li (2002) showed that Sr^{2+} can be incorporated between the sheet units in curite and becquerelite, and Cahill & Burns (2000) reported the structure of the Sr-containing mineral agrinierite. We will show here that adsorption of Sr^{2+} has a significant effect on the dissolution process of the basal face of curite.

Structure, Occurrence and Morphology of Curite and Its Synthetic Sr-Analogue

Curite has the general formula $Pb^{2+}{}_{3+x}(H_2O)_2[(UO_2)_4O_{4+x}(OH)_{3-x}]_2$ (Li & Burns 2000). In its structure, the two crystallographically distinct U^{6+} cations are [6]- and [7]-coordinated by two apical uranyl O-atoms and four or five equatorial $(OH)^-$ and O^{2-} groups, respectively (Li & Burns 2000, Mereiter 1979, Taylor e*t al*. 1981). The crystal structure of curite has space-group symmetry *Pnam* (orthorhombic) with *a* 12.53–12.58, *b* 13.01–13.03 and *c* 8.39–8.40 Å. The variation in lattice constants are caused by different contents of Pb^{2+} in the interlayer, which are most likely balanced by the substitution $(OH)^- \leftrightarrow O^{2-}$ in the structural unit (Li & Burns 2000).

Figures 1a and 1b show parts of a (100) layer in curite, in which the pentagonal- and tetragonal-bipyramidal uranyl polyhedra share common edges and corners involving equatorial O^{2-} and $(OH)^-$ anions. The apical U = O bonds are not involved in linkage between uranyl polyhedra, and point up and down into the inter-

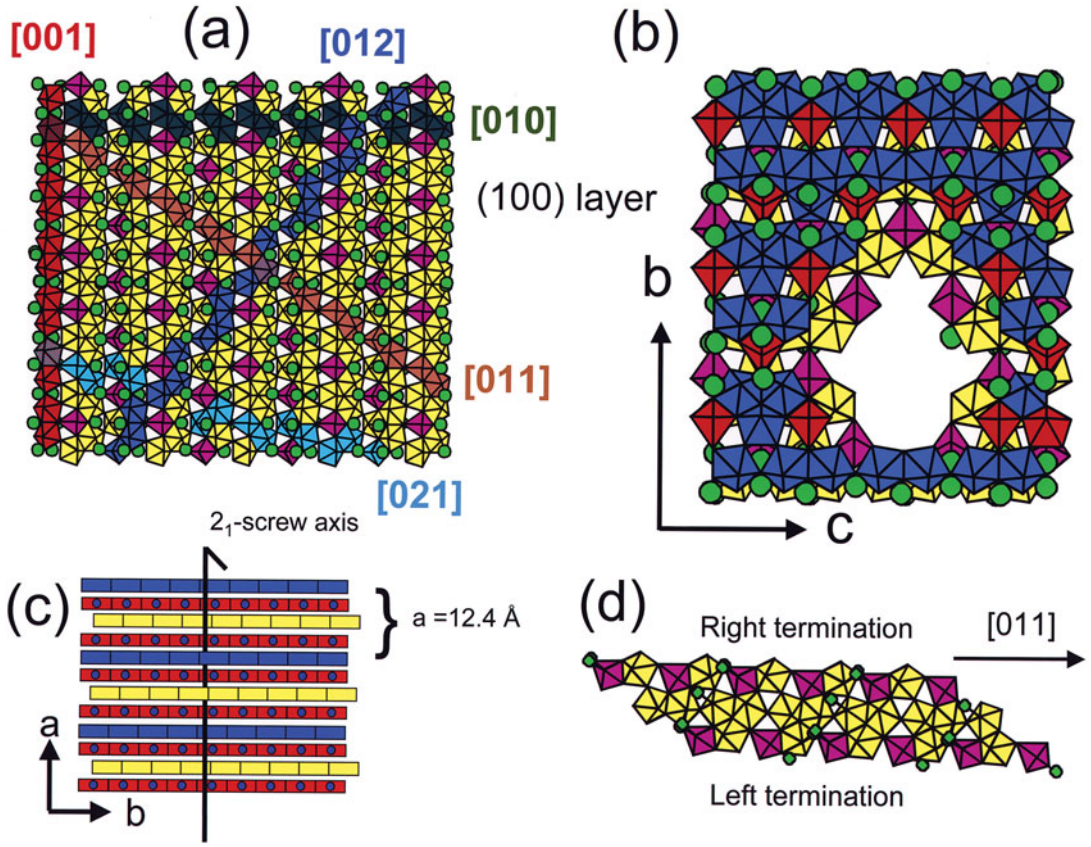

FIG. 1. (a) Polyhedron representation of the uranyl-hydroxy-hydrate sheet in curite. The polyhedron chains parallel to [001], [010], [012], [011] and [021] are highlighted in red, dark green, dark blue, brown and light blue, respectively; interstitial Pb^{2+} is indicated as green circles. (b) The polyhedron model of an etch pit showing the shift between adjacent layers and the different terminations of parallel chains of polyhedra in two consecutive layers. (c) A schematic sketch of layers and interstitial complexes in the (*ab*) plane; different orientations of the uranyl layers are indicated with blue and yellow blocks, and interstitial complexes are indicated by red blocks with blue circles; a two-fold screw axis parallel to *a* relates adjacent layers. (d) A polyhedron representation of the two different terminations of a [011] polyhedron chain (see text for more details).

stices. The additional Pb^{2+} atoms and (H_2O) groups occur between the layers (Figs. 1a, b). Burns & Hill (2000) reported the structure of a synthetic Sr-analogue of curite, $Sr^{2+}_{2.82}(H_2O)_2[(UO_2)_4O_{3.82}(OH)_{3.18})]_2$ with space-group symmetry *Pnam* and Sr^{2+} in positions similar to those of the Pb^{2+} atoms in curite.

Morphology and occurrence

Curite is a common product of oxidation, dissolution and replacement of uraninite (Isobe *et al*. 1992, Finch 1994). It is commonly associated with uranyl phosphate minerals, and several authors have proposed a genetic relation between these minerals (Frondel 1958, Deliens 1977, Finch & Ewing 1992). Figures 2a and 2b show the typical morphology of synthetic curite crystals, a prominent (100) face elongate along [001]. The edges defining the (100) face commonly have the indices [011], [0*kl*], $k < l$ and [001]. Natural curite crystals are more elongate along [001], forming needles up to several millimeters long, and the (100) basal face is defined only by the [011] and [001] edges (Schindler *et al*. 2004b).

PREDICTION OF THE CRYSTAL MORPHOLOGY AND THE MORPHOLOGY OF ETCH PITS IN CURITE

The growth and dissolution of minerals with sheet structural-units are strongly controlled by the reactivity of the edges along the basal face (Rufe & Hochella 1999). Schindler *et al*. (2004a) developed a new approach to evaluate the stability of edges on basal faces of uranyl-sheet minerals. They showed that the

occurrence of edges on basal faces depends on the interaction of the corresponding anion-terminations with the aqueous solution at different pH and degrees of supersaturation. The degree of interaction between the anion terminations on an edge and the species in aqueous solution is controlled by (1) the number of kink sites and the chemical composition of the chains of polyhedra parallel to the edge, (2) the arrangement of the interstitial complexes, and (3) the displacement between adjacent layers. On the basis of these parameters, Schindler *et al.* (2004b) predicted the occurrence of edges on the basal faces of uranyl-sheet minerals and compared them with observations on minerals and synthetic compounds. They further used this approach to develop a mechanism of crystal growth of uranyl-hydroxy-hydrate minerals such as schoepite, $[(UO_2)_8O_2(OH)_{12}](H_2O)_{12}$, becquerelite, $Ca[(UO_2)_3O_2(OH)_3]_2(H_2O)_8$ and wyartite, $Ca[U^{5+}(UO_2)_2(CO_3)\ O_4(OH)](H_2O)_7$ on the (104) surface of calcite (Schindler & Putnis 2004, Schindler *et al.* 2004c).

Structural and chemical composition of chains of polyhedra in the curite sheet

Depending on pH and the composition of the ambient solution, anions on the surface will be protonated or accept bonds from aqueous species such that they obey the valence-sum rule (Brown 1981, Hawthorne 1994, 1997). Protonation and acceptance of bonds from aqueous species are the results of interaction of a surface anion with the aqueous solution. One can express the interaction of anions at an edge with the aqueous solution by their bond-valence deficiency (calculated for no interaction with the aqueous solution) along a terminating chain of polyhedra parallel to a specific edge (Schindler *et al.* 2004a) . Chains with the lowest bond-valence deficiency are chains in which the anions have the lowest interaction with the aqueous solution. An edge parallel to a chain with the lowest bond-valence deficiency has the highest stability and most likely will occur on the final morphology of the crystal or etch pit.

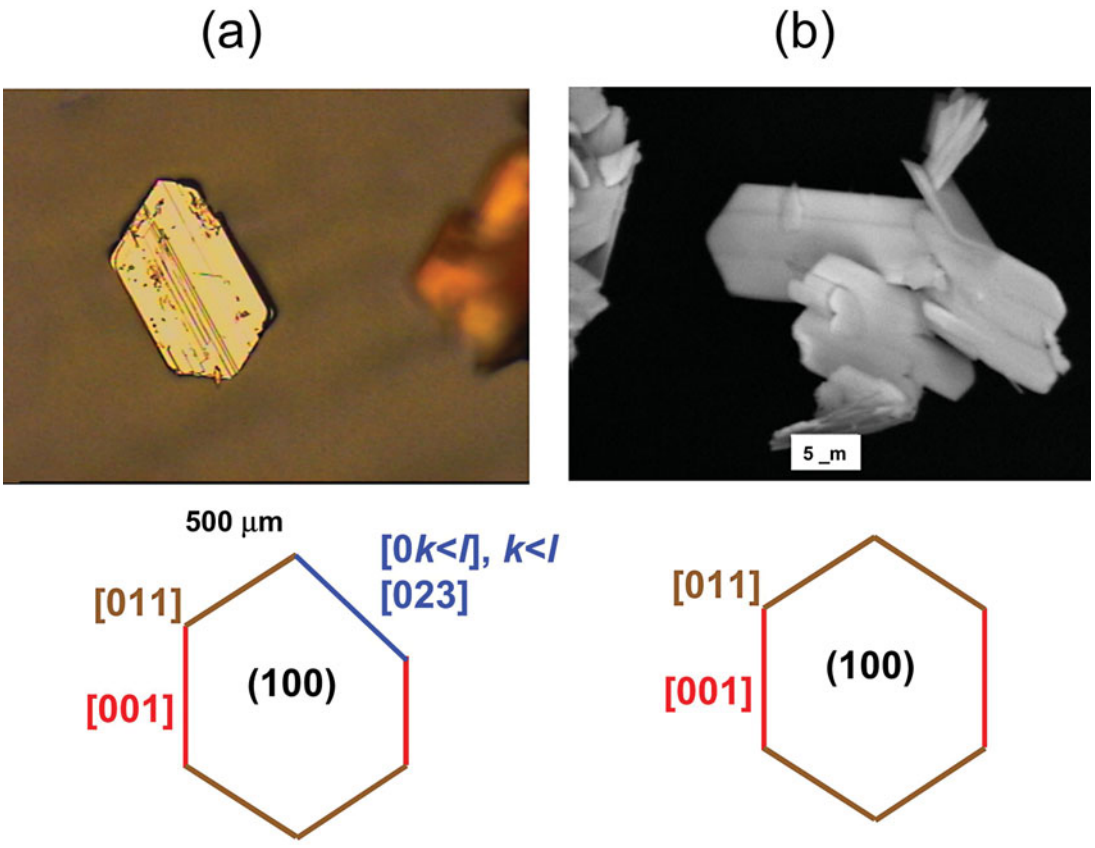

FIG. 2. (a) Synthetic crystal of curite with a prominent (100) face defined by the [001], [011], [100] and [023] edges. (b) SEM image of synthetic crystals of curite; the basal face is defined by the [011] and [001] edges.

There are in some cases more than one type of polyhedron chain parallel to an edge (an exact definition of a polyhedron chain is given by Schindler *et al*. 2004a). These different types of polyhedron chains are numbered 1, 2, 3... and plotted against their bond-valence deficiency. However, one only considers the lowest bond-valence deficiency for a set of polyhedron chains parallel to the same edge and compares this value with the lowest bond-valence deficiency of a set of polyhedron chains parallel to another edge.

Figures 3a and 3b show the variation in bond-valence deficiency (in valence units, *vu*) per unit length [*vu*/Å] of anions along different chains parallel to edges defining the (100) face of curite. There are two distinct polyhedron chains parallel to each edge, which means that the polyhedron chains "1" and "3" are identical through the translation period perpendicular to the edge. The bond-valence deficiencies were calculated using the average bond-valence for $^{[6]}$U–ϕ, $^{[7]}$U–ϕ, and O–H bonds of 0.72, 0.58 and 0.80 *vu*, respectively. The values for $^{[n]}$U–ϕ were calculated from the average U–O bond lengths of Li & Burns (2000) using the bond-valence parameter for $^{[6]}U^{6+}$ and $^{[7]}U^{6+}$ from Burns (1999). The bond valence of the O–H bond is an average value in inorganic structures (Brown 1981).

Figures 3a and 3b indicate that a chain of polyhedra can have different bond-valence deficiencies on its right and left terminations. This can be explained with the type and number of different anion-terminations on the left and right terminations of polyhedron chains. For example, the chain of polyhedra parallel to [011] has different left and right terminations, *i.e*., the left termination has in its repeat length the anion terminations 2 × $^{[6]}$U–O, 2 × $^{[6]}$U–O–$^{[7]}$U, and 2 × $^{[7]}$U–OH, whereas the right termination has in its repeat length the anion terminations 2 × $^{[7]}$U–O, 2 × $^{[6]}$U–OH–$^{[7]}$U, and 2 × $^{[6]}$U–O–$^{[7]}$U (Fig. 1d). Hence, there is a lower number of $^{[m]}$U–ϕ terminations on its right termination than on its left termination. This results in a lower bond-valence deficiency along the right termination than along the left termination.

In *Pnam*, a two-fold screw axis parallel to [100] relates adjacent sheets by 180° rotation and translation by *a*/2 (Fig. 1c). Hence, left and right terminations of each chain of polyhedra chain occur along the same edge (Fig. 1b), and their different degrees of interactions with the aqueous solution can be combined. Inspection of Figures 3a, b shows that the interaction of an edge with the aqueous solution increases in the following sequence: [001] < [011] = [0*kl*], $k < l$, [010] = [0*kl*], $k > l$.

Displacement between the sheets and arrangement of interstitial complexes

Schindler *et al*. (2004a) showed that any displacement between layers in a uranyl-sheet mineral increases the interaction between an edge and aqueous species in solution. In curite, every second layer is slightly displaced along [010] relative to the first layer (Figs. 1b, c), which may have only a minor effect on the stability of the edges. Schindler *et al*. (2004a) also showed that the arrangement of interstitial complexes in rows parallel to specific edges favors growth of the crystals in the same direction. In curite, the interstitial complexes are arranged parallel to the [001] edge, in accord with the common acicular habit of curite.

On the basis of the calculated bond-valence deficiencies, the displacement between the layers and the arrangement of cations, the [001] edge should be the dominant edge on the basal face and etch pits, and edges such as [011] and [0*kl*], $k < l$, should terminate the elongate crystals and etch pits. This prediction is in agreement with observations on natural and synthetic crystals (see above, Figs. 2a, b, c, d, and Schindler *et al*. 2004a).

Experimental

Synthesis of curite

Following the procedure of Li & Burns (2000), curite was synthesized by combination of 20 mL of a 0.1 mol L^{-1} uranyl acetate solution and 20 mL of a 0.1 mol L^{-1} $Pb(NO_3)_2$ solution, and subsequent heating at 220°C for two weeks in Teflon Parr bombs. The X-ray powder-diffraction pattern of the well-crystallized product did not indicate the presence of any phases other than curite.

Dissolution experiments

In the dissolution experiments, we combined 70 mg of single crystals of curite with 50 mL of doubly distilled water. Solutions with pH values of 3.5 and 2.1 were prepared by adding drops of a 6 mol L^{-1} HCl solution (uncertainty in pH values is ±0.1). Weakly and strongly acidic solutions containing Sr were prepared by combining 70 mg of curite crystals with 70 mL of a 0.50 mol L^{-1} $SrCl_2$ solution and with drops of a 6 mol L^{-1} HCl solution. The initial values of pH of these solutions were 5.5 and 2.7, respectively. A dissolution experiment under basic conditions (pH = 10.5) was done by combining 70 mg of curite crystals with 50 mL of a 0.1 mol L^{-1} Na_2CO_3 solution. After the dissolution experiments, the pH values of all solutions were similar (±0.5) to the initial pH values. In order to form etch pits, it was necessary to heat all solutions in Teflon Parr bombs at 60°C for 24 h. Afterward, the crystals were washed in distilled water, dried in air and mounted for atomic force microscopy.

Atomic-force microscopy

After the dissolution experiments, the (100) surface of curite was examined with a Nanoscope III and

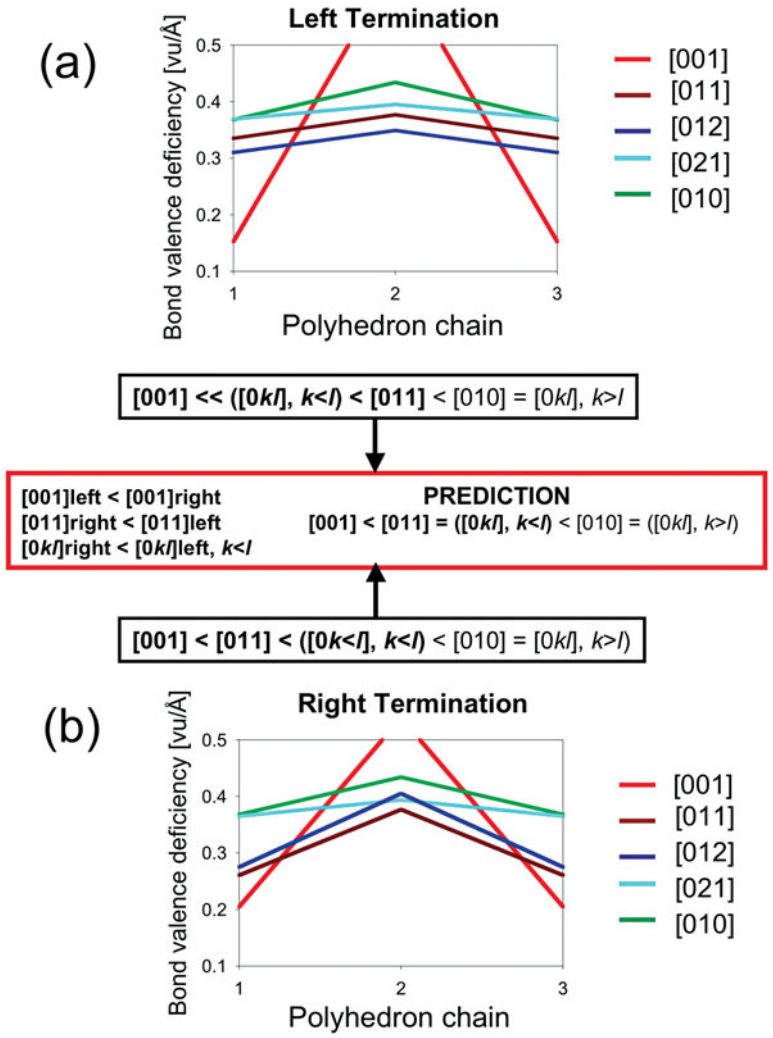

FIG. 3. (a), (b) Calculated bond-valence deficiencies of the left and right forms of terminations on polyhedron chains parallel to the edges [001], [010], [011], [012] and [021].

a Dimensional 3000 atomic force microscope from Digital Instruments. The surface was scanned with a standard silicon nitride (Si_3N_4) contact-mode tip in air. In order to verify that the contact mode and scanning direction did not affect shape and orientation of the etch pits, we invariably scanned an area at least twice in orthogonal directions. The AFM images were subsequently analyzed and modified with the software package of Digital Instruments. Images taken in deflection mode were modified with the FLATTEN and PLANEFIT procedures, which correct the images for sample tilt, linear and oscillating drifts. Images in deflection and height mode were also modified with the *zoom* option of the AFM software.

RESULTS

Figure 4a shows an AFM image of three characteristic etch-pits on the (100) surface of curite after dissolution in water. Figures 4b and 4c show in more detail the morphology of two of these three etch-pits: different colors indicate different depths. The crystallographic orientation of the etch pits is indicated in Figure 4d, which shows that the edges [001], [011] and [0*kl*], $k < l$ define the morphology of the etch pits. The latter edge makes an angle of 51° with the [001] edge, which indicates that the edge is parallel to [012]. We did not assign any [*uvw*] indices to the edge at the lower right of the etch pit because of its rounded shape.

The morphology of the etch pits changes with depth. At greater depth, only [011] and [0*kl*], $k < l$, edges define the morphology of the pits, whereas the length of the [001] edge increases with decreasing depth.

Dissolution in solutions of pH 3.5 and 2.1

Figure 5a shows an AFM image of etch pits on the (100) face of curite after 12 h contact time with a solution of pH 3.5. The pit is slightly more elongate in the plane of the crystal surface than the etch pits formed in water. The angle between the [001] and [0*kl*], $k < l$, edges on the right termination (the deeper part of the etch pit) is now 57°, which indicates that both edges are parallel to [011] (Fig. 5b). The left termination of the etch pit is more rounded than the right termination. However, straight edges parallel to [011] and [056] may be assigned to parts of the curved termination. The length of the [001] edge increases with decreasing depth of the etch pits, similar to etch pits formed in water.

Figure 5c shows an AFM image of an etch pit on the (100) face of curite after contact with a solution of pH = 2.1. The elongate etch-pit is defined by rounded edges parallel to the elongation, and is terminated by [001] edges. The depth of the etch pit is nearly constant, indicating no change in morphology with decreasing depth (Fig. 5d). The angle between the rounded edges and the [001] edge is approximately 75°.

Comparison of the morphology of the etch pits indicates that the angle between the [001] and [0*kl*], $k < l$, edges on the deeper side of the pits increases from 51° to 57° to 75° with decreasing pH of the solution. Furthermore, the length of the [001] edge at the upper layer of the etch pit increases with decreasing pH (Figs. 6a, b, c, right).

Cross sections of etch pits

Figures 6a, 6b and 6c show sections of etch pits formed in doubly distilled water and at pH 3.5 and 2.1,

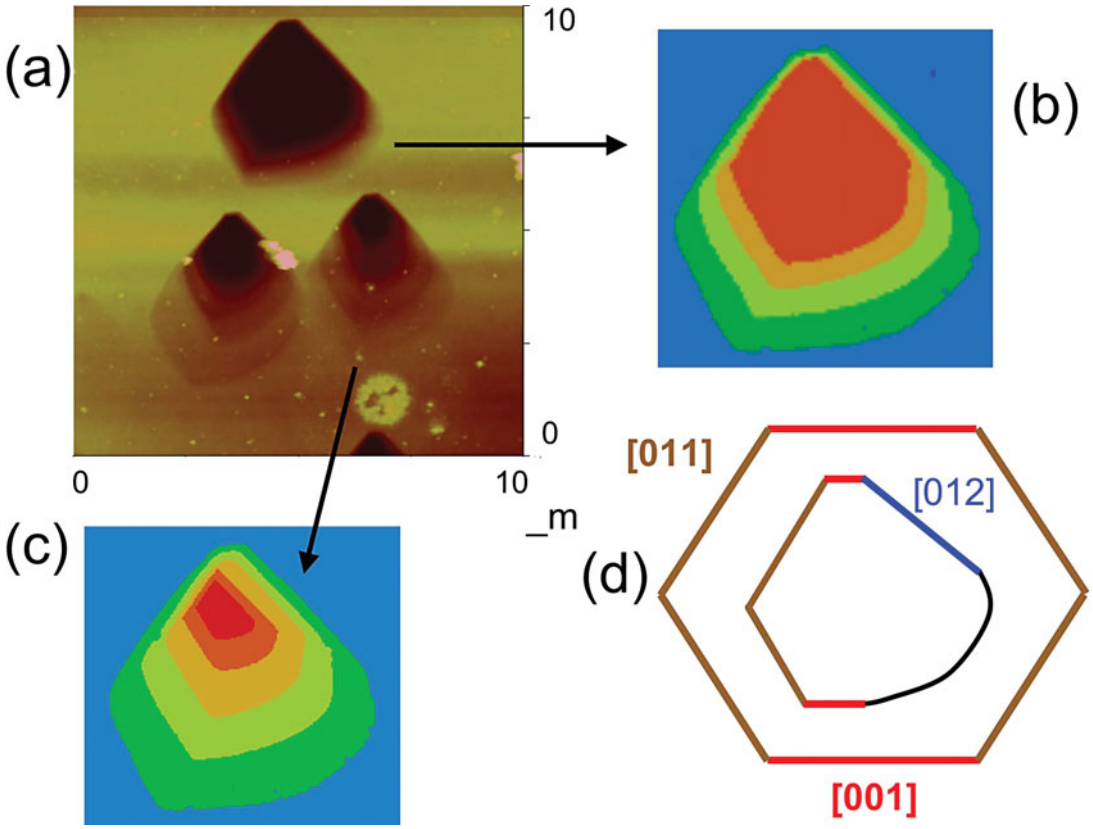

FIG. 4. (a) AFM images in height mode of etch pits formed on the curite (100) surface in water. (b), (c) The morphology of the etch pits, with different depths indicated with different colors. (d) The orientation of the etch pits in relation to the crystal morphology and the [*uvw*] indices of the edges.

respectively. These cross-sections were taken parallel to the [010] edge (which is approximately parallel to the elongation of the etch pits). In the cross-section of the etch pit formed in doubly distilled water, the sides are very asymmetrical. A steep edge at one side of the pit reaches a pronounced maximum depth close to that edge. Toward the center of the pit, it shallows rapidly with a convex surface and eventually merges with the surface (Fig. 6a, left). At pH 3.5, the leading edge of the pit is still steep, but the bottom of the pit is broader, the pit shallows away from the bottom less rapidly, and it has a slightly concave surface as it shallows (Fig. 6b, right). At pH 2.1, the bullet-shaped pit is shallower than the etch pits formed at higher pH; the bottom of the pit is flat and extends across almost the complete width of the pit (Fig. 6c, left).

Dissolution in weak acidic and strong acidic $SrCl_2$ solutions

Figure 7a shows an AFM image of a large etch-pit formed in 0.50 mol L^{-1} $SrCl_2$ at pH 2.7. The etch pits are defined by the [011], [0*kl*], $k < l$ and [001] edges, and the ratio of the lengths of the edges is similar at different depths of the pit. The boundaries of the etch pits resemble the boundaries of the faces on which they occur. However, the [001] edges are only partly developed, and one of the edges parallel to [001] is much shorter than the other (Fig. 7b). The bottom of the pit is flat over ~80% of the width of the pit, and the leading edge of the pit is steep but shallows away from the bottom with a slightly concave surface (Fig. 7c).

Figure 7a shows (in a small white frame) small etch-pits between the large etch-pits. These etch pits are

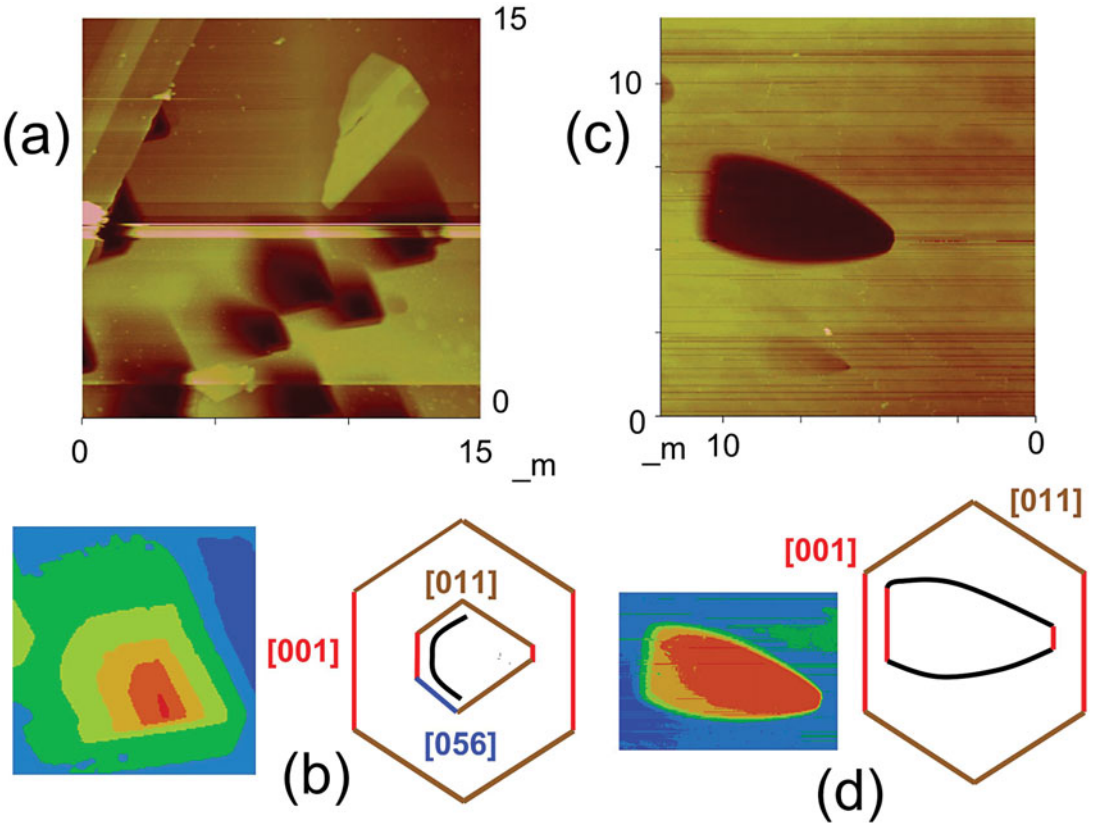

FIG. 5. (a), (b) AFM images in height mode of etch pits on the curite (100) surface formed in an HCl solution of pH 3.5, showing the change of their morphology at different depths, and their orientation relative to the crystal morphology. (c), (d) AFM images in height mode and cross-sections of etch pits on the (100) surface of curite, formed in an HCl solution of pH 2.1, showing the change of their morphology at different depths, and their orientation in relation to the morphology of the crystal.

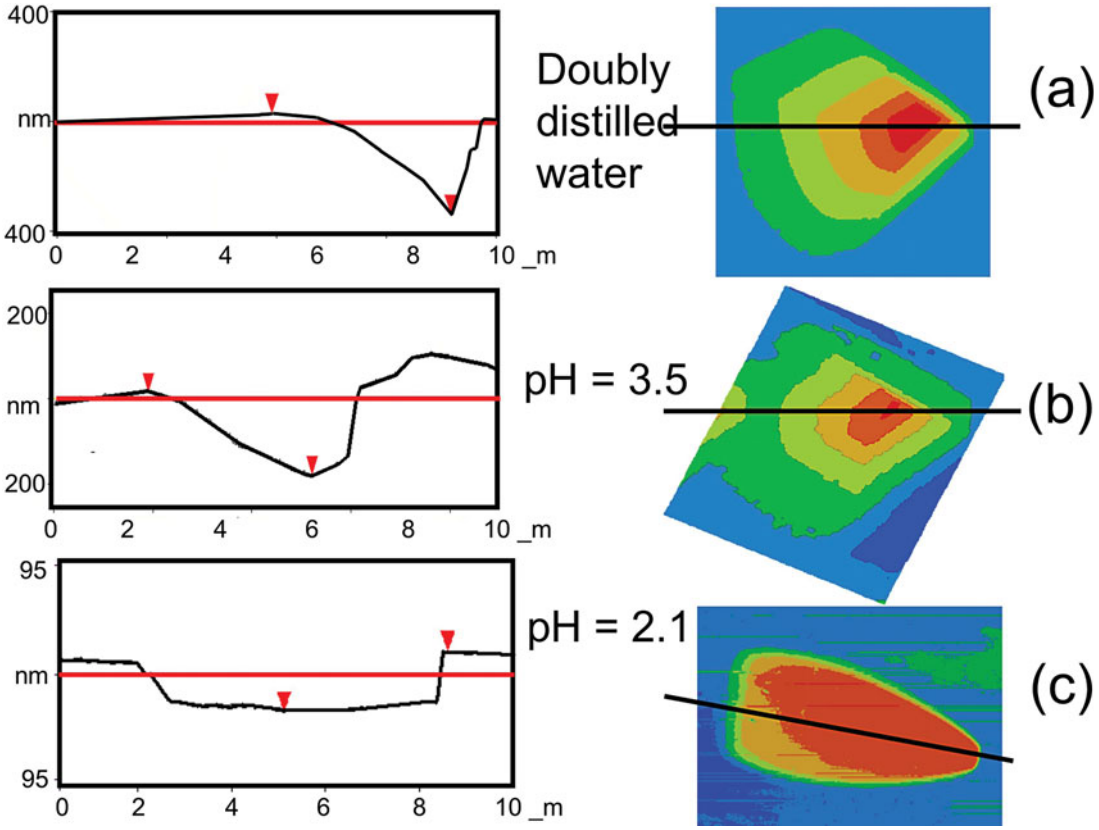

FIG. 6. Left: Cross sections of etch pits formed (a) in doubly distilled water, (b) in an HCl solution of pH 3.5, and (c) in an HCl solution of pH 2.1. Right: the corresponding etch-pits and the orientation of the cross sections in relation to etch-pit morphology (black lines).

elongate parallel to [001], are defined by a straight edge on the right side and by curved edges on the left side of Figure 7d, and are very shallow, with a maximum depth of 10 unit cells (~12.5 nm) (Fig. 7d). Their morphology and the morphology of etch pits of intermediate size suggest that the small etch-pits are most likely the earliest growth-stage of etch pits formed in $SrCl_2$ solution at pH 2.7. Scans of a surface treated with a weakly acidic $SrCl_2$ solution of pH 5.8 showed very few etch-pits; only three were found on the crystal, and their morphology is similar to that of etch pits formed in acidic solution of pH 2.7.

Dissolution in a 0.1 mol L^{-1} Na_2CO_3 solution

No etch pits were observed after submersion in a 0.1 mol L^{-1} Na_2CO_3 solution. Instead, we observed elongate prismatic hillocks parallel either to [011] (not shown) or to [023] (Figs. 8a, b). Atomic force microscopy and reflected-light microscopy did not show unequivocally if these hillocks are products of swelling or precipitation. The hillocks on the (100) surface of curite are defined by [011], [0*kl*], $k < l$ and [001] edges, and the upper terminations of the hillocks are rounded (Fig. 8b). The height of these hillocks averages 20 nm, and their maximum height does not exceed 100 nm.

DISCUSSION

All etch pits and hillocks on the (100) surface of curite are bounded by the [001], [011] and [0*kl*], $k < l$ edges, in agreement with our predictions. The occurrence of the [001] edge on surface features from the experiments in doubly distilled water and at pH 3.5 is restricted to the upper parts of the etch pits, where there has been more extensive lateral dissolution than in the deeper parts. This fact implies that during growth of etch pits parallel to the (100) surface, the rate of dissolution perpendicular to the [011] and [0*kl*], $k < l$ edges is larger than that perpendicular to the [001] edge, in

accord with the observed bond-valence deficiencies at all three edges. Hence, the [001] edge becomes larger with continued growth of etch pits parallel to the surface of the crystal. Figures 6a, 6b and 6c (right) show that with increasing protonation of the edges, the [001] edge becomes dominant, and the [011] and [0*kl*], $k < l$ edges finally disappear, again in agreement with our predictions. The [011] and [0*kl*], $k < l$ edges are still present at pH 3.5, but do not develop under more strongly acidic conditions, at pH 2.1. The degree of protonation and thus the interaction of the edges with the solution increases rapidly between pH 3.5 and pH 2.1.

Comparison of small and large etch-pits formed in the $SrCl_2$–HCl experiment indicates the differential development of edges during growth of the pits (Fig. 7). The [011] and [0*kl*], $k < l$ edges define the morphology of the large etch-pits, but do not occur in smaller etch-pits. This situation is in contrast to the [001] edge, which exists from the earliest stage of growth (on one side of the pit). This observation suggests that the [011] and [0$k < l$] edges form during lateral growth of the etch pit. Furthermore, the general occurrence of edges on the etch pits does not seem to vary with change in pH. Both observations must be related to the presence of Sr in the solution, a topic to be discussed below.

Dissolution rates perpendicular to edges and sheets

Dislocation defects induce strain energy in crystals, which is the energetic driving force for etch-pit formation. An etch pit involves both the formation of a deep hole and the spreading of stepwaves from the boundaries of the etch pits (Lasaga & Lüttge 2001). The spreading rate of a stepwave depends on the dissolution rate perpendicular to each edge, which can be expressed by either the retreat velocity of steps with identical heights or the lowering of the surface *versus* an unchanged reference-point on that surface. Here, the area of the upper layer of an etch pit (in $[\mu m]^2$) may indicate the general stability of an edge, and the depth of an etch pit (in [*nm*]) may express the change in relief of an etch pit *versus* its surrounding surface. This change in relief depends on the ratio between the lowering of the surrounding surface and the growth of an etch pit perpendicular to the basal face.

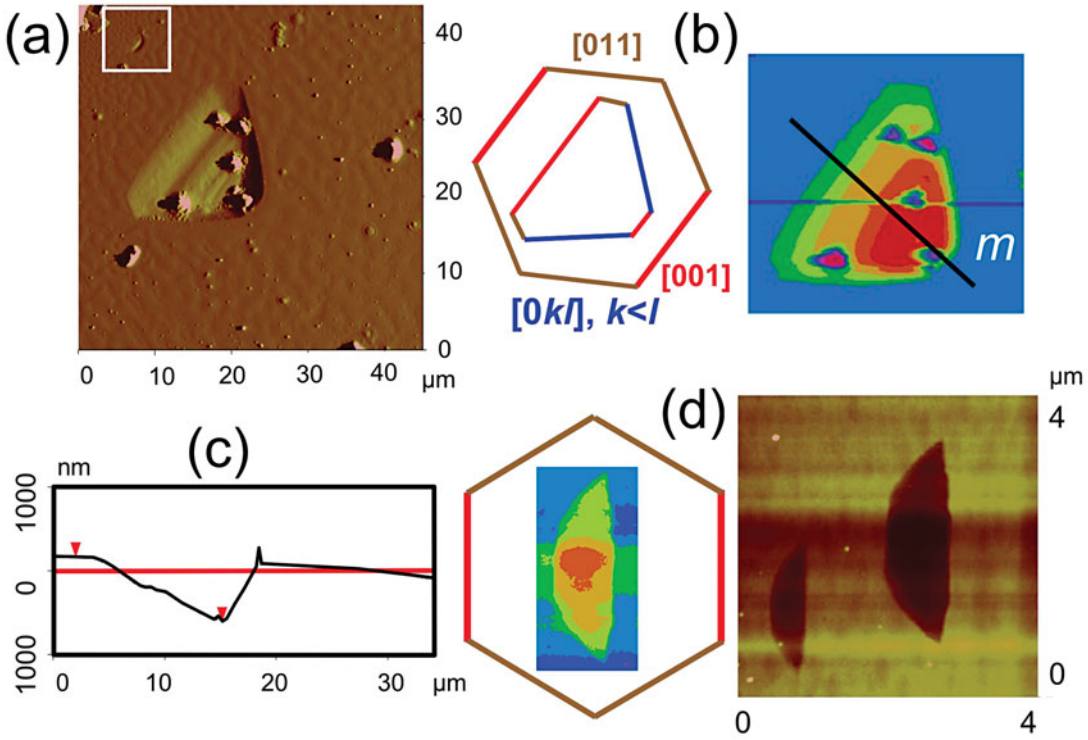

FIG. 7. (a) AFM image in deflection mode, of an etch pit formed in a $SrCl_2$–HCl solution of pH 2.7. (b) The orientation of the etch pit in relation to crystal morphology, and the morphology of the pit at different depths. (c) The cross section perpendicular to [001]. (d) AFM image in height mode showing the morphology and orientation of small elongate etch-pits framed in a white square box in (a).

For each sample, we examined etch pits on different areas of different crystals in order to collect a representative set of data. Data were excluded for etch pits that show intergrowth or occur along steps or terraces (*e.g.*, Fig. 5a), because these factors would have changed the growth of an individual etch-pit. The lateral area and the depth of an etch pit were determined by examination of two orthogonal cross-sections and plotted against each other (Fig. 9a).

Figure 9a shows the correlation between the dissolution rates perpendicular to edges (area) and the change in relief of the etch pits (depth) formed in the different experiments. It is apparent that at higher pH (*i.e.,* lower degree of protonation), the change in relief of an etch pit (*versus* the surrounding surface) is greater, whereas at lower pH (*i.e.,* higher degree of protonation), the dissolution rate perpendicular to an edge is greater. This phenomenon can be observed also in the cross-sections of the etch pits formed in distilled water and at pH 3.5 and 2.1 (Figs. 6a, b, c), where the different ratios of depth to lateral dimension are apparent.

The change in lateral dimensions and relief is a result of the differences in interaction of the edges with aqueous species at different pH. At high pH, the degree of protonation of the edges is lower, and their general stability is therefore higher than at lower pH. The higher stability of an edge at high pH prevents lowering of the surrounding surface, which increases the relief of the etch pit. Hence, the higher relief of an etch pit at high pH expresses a high ratio between the growth of an etch pit perpendicular to the sheet and the lowering of the surrounding surface.

We also observed a higher density of etch pits on curite surfaces that have been treated with solutions of higher acidity; *e.g.,* HCl: pH 2.1. The equilibrium constant for the dissolution reaction of curite has not been determined, but solubility measurements of uranyl-hydroxy-hydrate minerals indicate higher solubilities under strongly acidic and strongly basic conditions than under weakly acidic and weakly basic conditions (*e.g.,* Torrero *et al*. 1994, Casas *et al*. 1997). However, hillocks instead of etch pits form on the surface of curite in strongly basic solution. Dissolution experiments on the basal face of becquerelite, $Ca[(UO_2)_3O_2(OH)_3]_2(H_2O)_8$, showed similar results: at similar degrees of undersaturation, etch pits form under strongly acidic conditions, and hillocks form under strongly basic solutions (Schindler *et al*., in prep.). These observations suggest that the formation of etch pits on the basal surfaces of uranyl-oxide minerals depends more on the degree of protonation of the terminations on the basal face and its edges than on the degree of undersaturation with respect to the mineral. However, increase in etch-pit density with decreasing pH may be also a result of a higher degree of undersaturation with respect to curite. This would be in agreement with the general observation that the formation of etch pits correlates with the degree of undersaturation in solution (*e.g.*, Lasaga 1983).

Dissolution rates in aqueous $SrCl_2$–HCl solutions

There is an interesting correlation between the dissolution rates perpendicular to edges and to the sheet for etch pits formed in an aqueous $SrCl_2$–HCl solution at pH 2.7 (Fig. 9b). The small etch-pits have nearly identical areas but vary in depth. This behavior contrasts with that of the larger etch-pits, which vary in both area and depth (Fig. 9b). At the earliest stage of growth, etch pits of equal lateral dimensions thus grow perpendicular to the sheet until they reach a critical depth, at which they extend laterally with only

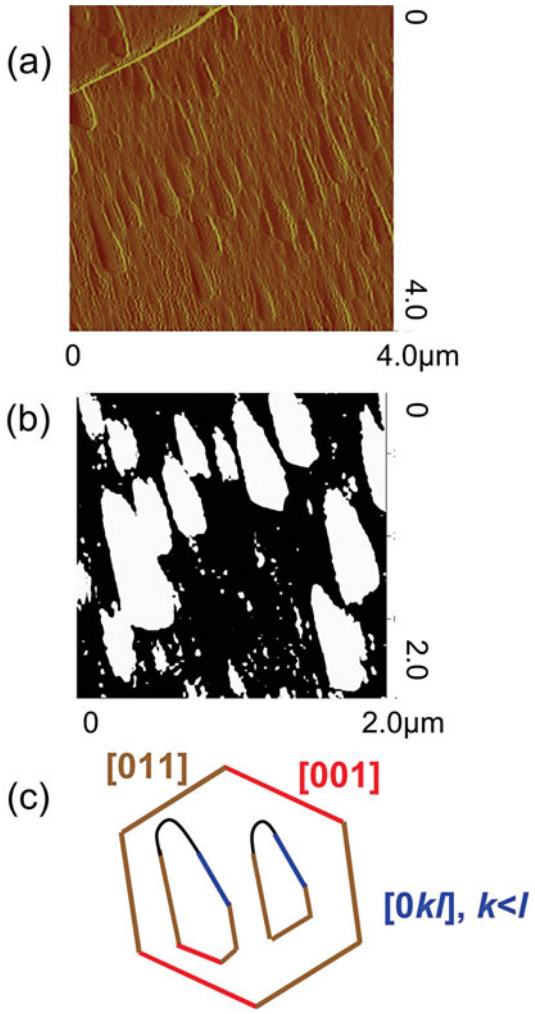

FIG. 8. (a) AFM images in deflection mode, of hillocks on the (100) surface of curite formed in an Na_2CO_3 solution of pH 10.5. (b) AFM images in height mode, of the hillocks showing details of their morphology. (c) the orientation of the hillocks with respect to the crystal morphology.

minor growth perpendicular to the sheet (relative to the surrounding surface).

Symmetry Elements and Structural Models

Prior to the widespread use of diffraction methods, the symmetry of etch pits was used to determine the symmetry of minerals (*e.g.*, Honess 1927). The structure of curite has space-group symmetry *Pnam*: a two-fold screw axis is perpendicular to the basal face, and a mirror plane is perpendicular to the *c* axis. Which symmetry can we expect for etch pits grown on the basal face of curite?

In order to answer this question, we have to consider at first a mineral with a similar arrangement of symmetry elements perpendicular to one of its prominent faces. A good example is barite, $BaSO_4$, where the structure also has space-group symmetry *Pnam* and where a two-fold screw axis and a mirror plane are perpendicular to its prominent (001) face. The dissolution of barite has been studied extensively because of its precipitation in pipes during offshore exploration for oil. *In situ* AFM observations show that triangular etch-pits with a lateral dimension of ~1 μm and a depth of one half of a unit cell form on the (001) surface in the first minutes of contact with pure water (Risthaus *et al*. 2001, Becker *et al*. 2002). Furthermore, etch pits in consecutive atomic layers have orientations that are symmetrically related by the two-fold screw axis. Moreover, the triangular etch-pits have two equal sides symmetrically related by a mirror plane. Optical examination of etch pits formed over a longer period indicates that they are rectangular in outline (upper micrometer range) and that these etch-pits display plane-group symmetry *mm2* (Honess 1927).

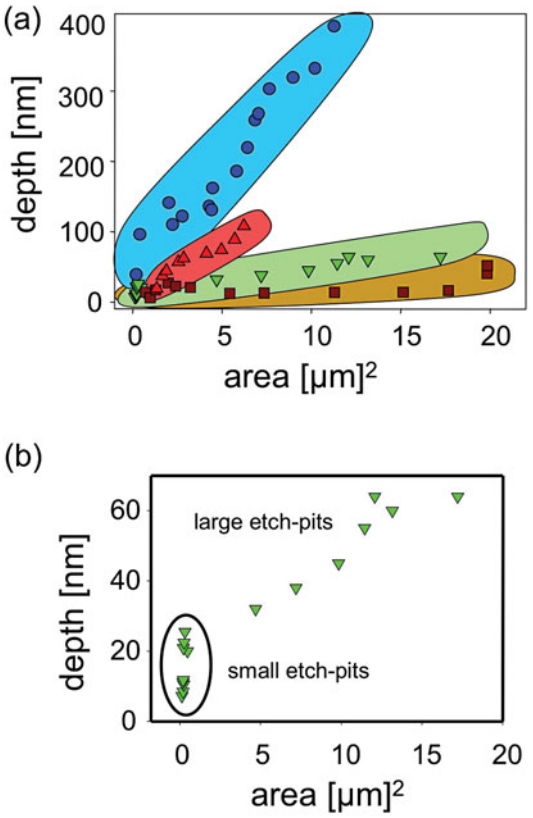

FIG. 9. (a) The variation in depth [nm] *versus* the variation in the lateral dimension [μm^2] for etch pits formed in water (blue circles), in an HCl-solution of pH 3.5 (red triangles pointing up), in a $SrCl_2$ solution of pH 2.7 (light green triangles pointing down), and in an HCl solution of pH 2.1 (brown squares). (b) The same correlation as in (a), but only for etch pits formed in a $SrCl_2$–HCl solution of pH 2.7.

The morphology and arrangement of etch pits formed on the (100) face of curite in doubly distilled water show none of these symmetry elements; they do not have mirror symmetry, and etch pits at different heights on the surface invariably have the same orientation (Figs. 4, 5, 10a). We have never observed etch pits with opposite orientation (*i.e.*, symmetrically related by the two-fold screw axis) on the (100) surface of curite. Considering the dissolution experiments without Sr, only the etch pits formed at pH 3.5 have nearly identical angles between the [0*kl*] and [001] edges, a requisite for mirror symmetry perpendicular to [001] (Figs. 5a, b). The morphology of small and large etch-pits formed in an aqueous $SrCl_2$–HCl solution invariably shows mirror symmetry perpendicular to [001] (Figs. 7b, 10c). The morphology and orientation of the hillocks do not show any indication of a two-fold screw axis parallel to the *a* axis or of a mirror plane perpendicular to the *b* and *c* axes (Fig. 8).

Structural model of etch pits formed in water at pH 5.0

The occurrence and development of an edge depend on its interaction with the species in solution, which correlates with the bond-valence deficiency of the corresponding chains of polyhedra (Schindler *et al*. 2004a). The asymmetry of the etch pits indicates that symmetrically related edges develop differently, *i.e.*, their corresponding chains of polyhedra have different bond-valence deficiencies. Right and left terminations of a chain parallel to the same edge differ significantly in bond-valence deficiency. We showed above that right and left terminations occur on two adjacent layers along the same edge. Hence, one would expect triangular etch-pits to have opposite orientations where displaced by an odd number of half-unit-cell displacements. However, this is not observed on the (100) surface of curite, an observation that seems to violate the crystallographic symmetry of the curite structure.

Right and left terminations of chains of polyhedra on the surface layer control the orientation(s) of the etch pits. This is indicated in a cross-sectional model of an etch pit (Fig. 10b), where green and red blocks indicate chains of polyhedra of left and right termination, respectively. The right termination of a polyhedron chain along the [011] edge has a lower bond-valence deficiency than the corresponding left termination (Figs. 3a, b). During dissolution of the surface layer, the dissolution rate perpendicular to the chain with the left termination is higher than that perpendicular to the chain with the right termination. Hence, the etch pit grows more rapidly perpendicular to the [011] and [0*kl*,], $k < l$ edges with left-terminated chains of polyhedra (Fig. 10b). The retreat of the surface layer produces a major kink-site between itself and the layer beneath. Hence, chains of polyhedra with right terminations in the layer beneath can be more easily attacked by aqueous species than the corresponding chains of polyhedra with left terminations, because the upper layer protects the latter polyhedra from attack by the species in solution. Continuous growth of the etch pit would result in a steep edge at the side involving the right termination of the layer and a convex surface with a high number of steps on the side involving the left termination of the layer. The slope of the convex surface on the left termination of the layer depends on the dissolution rate perpendicular to the edges, and hence depends on pH. For example, the higher rate of dissolution at lower pH produces steeper edges on both sides of a flat bottom of the etch pit, whereas at higher pH, only one of the edges is steep (Figs. 6a, b).

On the basis of this dissolution model, we assigned left and right terminations of the polyhedron chains to different edges at the surface layer of the structural model of the etch pit (Fig.10a). The assignment of left terminations of the [011] and [0*kl*], $k < l$ polyhedron chains is not only in agreement with the observed cross-sections, it also explains the rounded and less well defined edges on the rounded side of the etch pit.

The edge pits formed in aqueous $SrCl_2$ solutions also show only one orientation, and their cross-sections show steep edges and convex surfaces (Figs. 7a, b, c). Hence, the proposed model is also in agreement with the morphology and orientations of the etch pits formed in the presence of Sr^{2+}.

Non-stoichiometric detachment of polyhedra or groups of polyhedra

If polyhedra or groups of polyhedra detach stoichiometrically from a surface (such as in barite, Risthaus *et al*. 2001), the etch pits should obey the plane-group symmetry of the bulk structure. Thus, etch pits on the surface of barite show the symmetry of the bulk structure (Risthaus *et al*. 2001), except where inner-sphere complexes modify the stability of certain edges. The asymmetrical etch-pits observed in experiments without Sr^{2+} do not follow the symmetry of the bulk structure, which suggests a decrease in the symmetry of the surface structure during dissolution. The lower symmetry of the surface structure is most likely the result of a change in the chemical composition of the edges, which may be caused by non-stoichiometric detachment of their polyhedra ($Pb\phi_n$, $\{([6]UO_2)\phi_4\}$ and $\{[7](UO_2)\phi_5\}$ polyhedra; ϕ: undefined ligand).

Frondel (1958) and Finch & Ewing (1992) showed that the enrichment of Pb in corrosion rinds of uraninite is caused by the preferential loss of U to groundwater. The preferential loss of U, *i.e*., preferential detachment of U-polyhedra, would explain the observed asymmetrical etch-pits on the surface of curite. The corresponding dissolution of curite could be written as the following reaction:

$$\begin{aligned} &Pb^{2+}{}_3(H_2O)_2[(UO_2)_4O_4(OH)_3]_2 + x(10H_2O) \rightarrow \\ &Pb^{2+}{}_3(H_2O)_2[(UO_2)_{4-x}O_{4-x}(OH)_3]_2 \\ &+ x\{(UO_2)_3(OH)_5(H_2O)_5\}^+ \\ &+ x(5-2x)\ H^+ + x(H_2O) \end{aligned} \quad [1]$$

Occurrence of symmetrical etch-pits in the presence of Sr^{2+} cations in solution indicates that such change in chemical composition of polyhedron chains or interlayer is affected by adsorbed cations on the surface**.** These adsorbed cations could control the detachment of uranyl polyhedra through bonding to O atoms of their uranyl groups (as proposed by Schindler *et al*., in prep.).

The role of Sr^{2+} during dissolution

In order to understand the role of Sr^{2+} during dissolution, we have to consider the following points:

(1) Curite crystals formed in a Pb^{2+}-containing solution show point-group symmetry *mmm* and are elongate along [001];

(2) In the bulk structure of curite, interstitial Pb^{2+} are arranged in rows parallel to [001];

(3) Crystals of the Sr-analogue of curite (formed in a Sr^{2+}-containing solution) show point-group symmetry *mmm* and are elongate along [001];

(4) In the bulk structure of the Sr-analogue of curite, interstitial Sr^{2+} atoms occur at similar positions to Pb^{2+} in curite; *i.e*., they are also arranged in rows parallel to [001];

(5) In contrast to etch pits formed in HCl and H_2O solutions, etch pits formed in a Sr^{2+}-bearing solution display plane-group symmetry *m*, and their morphology is defined by a prominent [001] edge;

(6) Recent dissolution-experiments on the basal face of becquerelite, $Ca[(UO_2)_3O_2(OH)_3]_2(H_2O)_8$, in different electrolyte solutions show that etch pits are elongate parallel to the rows of cations in the bulk structure (which contains the cation of the electrolyte solution) (Schindler *et al*., in prep).

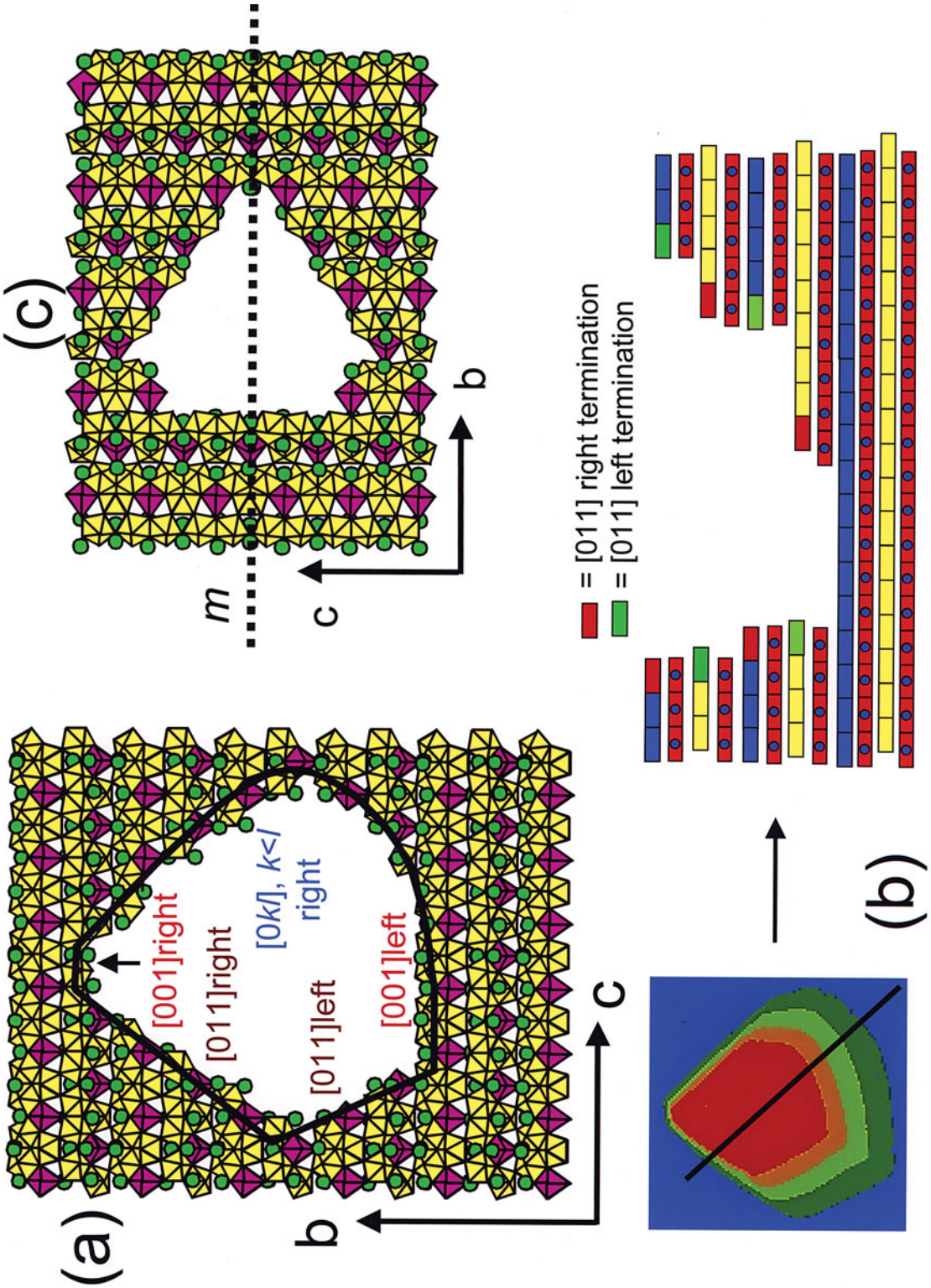
(a)
[001]right
[011]right
[0kl], k<l
right
[011]left
[001]left
b
c
(b)
= [011] right termination
= [011] left termination
(c)
m
c
b

These facts suggest that

(1) The formation of etch pits on the basal surface of curite in a Sr^{2+}-bearing solution is strongly controlled by the presence of Sr^{2+} on the surface of the basal face;

(2) The growth of crystals and etch pits is controlled by the arrangement of cations on the surface of uranyl-bearing minerals with sheets of polymerized uranyl-polyhedra.

Formation of hillocks under basic conditions

Aldushin *et al*. (2004a, b) observed hillocks on the basal face of sheet-silicate minerals ("apophyllite", biotite, phlogopite) during dissolution in an acidic solution. They interpreted the hillocks as a result of swelling during the release of interstitial cations from the interlayer. They argued that the swelling is a result of replacement of interstitial cations by $(H_3O)^+$ and the subsequent protonation of terminal O-atoms of the silicate sheet to form silanol groups. On the other hand, Kalinowski & Schweda (1996) attributed such swelling to the occurrence of "hydroxy interlayers". On the basis of *in situ* HAFM (Hydrothermal Atomic Force Microscope) observations on hillock growth on the basal face of "apophyllite", $KCa_4[Si_8O_{20}(F,OH)](H_2O)_8$, Aldushin *et al*. (2004a, b) showed that the formation and spread of hillocks increase with decreasing pH, and suggested that protons promote the formation of hillocks.

On the basal face of curite, hillocks form under basic conditions, whereas etch pits form in neutral, weakly and strongly acidic solutions. Recent dissolution-experiments on becquerelite showed that hillocks also occur under neutral and weakly acidic conditions, whereas etch pits form only in strongly acidic solutions. In the case of uranyl-hydroxy-hydrate minerals, the formation of etch pits *versus* hillocks is favored by increase in the degree of protonation of the surface species. As stated above, neither AFM nor reflected-light microscopy could show unequivocally if the observed hillocks on the basal surface of curite are products of swelling or precipitation.

FIG. 10. (a) Polyhedron representation of a structural model of an etch pit formed in water. (b) Schematic model of the cross section of an etch pit; the blue and yellow blocks represent layers of uranyl polyhedra of different orientation, the red and green blocks correspond to polyhedron chains with left and right terminations, and the red squares with blue circles indicate the interstitial complexes. (c) Polyhedron representation of an etch pit formed in $SrCl_2$–HCl solution of pH 2.7. The presence of the mirror plane perpendicular to the *c* axis is indicated by a dashed line.

SUMMARY

Dissolution experiments on single crystals of curite, followed by AFM examination of the (100) surface, has given significant insight into the mechanisms of dissolution in uranyl-oxide-hydroxy-hydrate minerals. Etch pits formed in distilled water and in HCl–H_2O solutions of pH 2.1 and 3.5 have lower relief and larger lateral dimensions at lower pH. Both changes in morphology indicate a lower stability of edges at lower pH, which suggests that different degrees in protonation of edges are the primary control on the dissolution rate of edges. The orientation of etch pits is controlled by the right and left terminations of chains of polyhedra on the surface layer, but the occurrence of only one orientation violates the presence of a two-fold screw axis in the symmetry of the bulk structure. The asymmetrical outline of the etch pits in the experiments without Sr^{2+} may be due to the non-stoichiometric detachment of uranyl polyhedra from the basal surface of curite. Dissolution experiments in an aqueous $SrCl_2$-bearing solution at pH 2.7 result in higher-symmetry etch-pits, which resemble the outline of the basal face of the curite crystals more clearly than the etch pits formed in solutions without Sr^{2+}. This observation shows that the presence of potential radionuclides in solutions could influence the dissolution rates of edges on the surface of uranyl minerals. The formation of hillocks under basic conditions indicates either a different mechanism of dissolution or process of precipitation than that operating at acidic conditions. The general occurrence of edges on etch pits and hillocks formed during dissolution are in agreement with the predictions of Schindler *et al*. (2004a).

ACKNOWLEDGEMENTS

This work was supported by a Canada Research Chair in Crystallography and Mineralogy, and Discovery, Major Facilities Access, and Research Tools and Equipment grants to FCH from the Natural Sciences and Engineering Research Council of Canada. We thank two anomynous reviewers, Associate Editor Dogan Paktunc and Editor Bob Martin for their comments on an earlier version of this paper.

REFERENCES

ABDELOUAS, A., LUTZE, W. & NUTALL, H.E. (1999): Uranium contamination in the subsurface: characterization and remediation. *In* Uranium: Mineralogy, Geochemistry and the Environment (P.C. Burns & R. Finch, eds.). *Rev. Mineral*. **38**, 433-473.

ALDUSHIN, K., JORDAN, G., RAMENSEE, W., SCHMAHL, W.W. & BECKER, H-W. (2004a): Apophyllite (001) surface alteration in aqueous solutions studied by HAFM. *Geochim. Cosmochim. Acta* **68**, 217-226.

ALDUSHIN, K., JORDAN, G., FECHTELKORD, M., SCHMAHL, W.W., BECKER, H.W. & RAMMENSEE, W. (2004b): On the mechanisms of apophyllite alteration in aqueous solutions. A combined AFM, XPS and MAS NMR study. *Clays Clay Minerals* **53**, 432-442.

BECKER, U., RISTHAUS, P., BOSBACH, D. & PUTNIS, A. (2002): Selective attachment of monovalent background electrolyte ions and growth inhibitors to polar steps on sulfates as studied by molecular simulations and AFM observations. *Molecul. Simul.* **28**, 607-632.

BROWN, I.D. (1981): The bond-valence method: an empirical approach to chemical structure and bonding. *In* Structure and Bonding in Crystals II (M. O'Keeffe & A. Navrotsky, eds.). Academic Press, New York, N.Y. (1-30).

BUCK, E.C., BROWN, N.R. & DIETZ, N.L. (1996): Contaminant uranium phases and leaching at the Fernald site in Ohio. *Environ. Sci. Technol.* **30**, 81-88.

BURNS, P.C. (1999): The crystal chemistry of uranium. *In* Uranium: Mineralogy, Geochemistry and the Environment (P.C. Burns & R. Finch, eds.). *Rev. Mineral.* **38**, 23-90.

BURNS, P.C., DEELY, K.M. & SKANTHAKUMAR, S. (2004): Neptunium incorporation into uranyl compounds that form as alteration products of spent nuclear fuel: implications for geologic repository performance. *Radiochim. Acta* **92**, 151-159.

BURNS, P.C., EWING, R.C. &MILLER, M.L. (1997): Incorporation mechanims of actinide elements into the structures of U^{6+} phases formed during the oxidation of spent nuclear fuel. *J. Nucl. Mater.* **245**, 1-9.

BURNS, P.C. & HILL, F.C. (2000): Implications of the synthesis and structure of the Sr analogue of curite. *Can. Mineral.* **38**,175-181.

BURNS, P.C. & LI, YAPING (2002): The structures of becquerelite and Sr-exchanged becquerelite. *Am. Mineral.* **87**, 550-557.

CAHILL, C.L. & BURNS, P.C. (2000): The structure of agrinierite: a Sr-containing uranyl oxide hydrate mineral. *Am. Mineral.* **85**, 1294-1297.

CASAS, I., BRUNO, J., CERA, E., FINCH, R.J. & EWING, R.J. (1997): Characterization and dissolution behaviour of a becquerelite from Shinkolobwe, Zaire. *Geochim. Cosmochim. Acta* **61**, 3879-3884.

CHEN, F., BURNS, P.C. & EWING, R.C. (1999): ^{79}Se: geochemical and crystallo-chemical retardation mechanisms. *J. Nucl. Mater.* **275**, 81-94.

CHEN, F., BURNS, P.C. & EWING, R.C. (2000): Near-field behavior of ^{99}Tc during the oxidative alteration of spent nuclear fuel. *J. Nucl. Mater.* **278**, 225-232.

DELIENS, M. (1977): Associations de minéraux secondaires d'uranium à Shinkolobwe (région du Shaba, Zaire). *Bull. Minéral.* **100**, 32-38.

FINCH, R.J. (1994): *Paragenesis and Crystal Chemistry of the Uranyl Oxide Hydrates*. Ph.D. thesis, Univ. of New Mexico, Albuquerque, New Mexico.

FINCH, R.J. & EWING, R.C. (1992): The corrosion of uraninite under oxidizing conditions. *J. Nucl. Mater.* **190**, 133-156.

FINCH, R.J. & MURAKAMI, T. (1999): Systematics and paragenesis of uranium minerals. *In* Uranium: Mineralogy, Geochemistry and the Environment (P.C. Burns & R. Finch, eds.). *Rev. Mineral.* **38**, 91-180.

FINN, P.A., HOH, J.C., WOLF, S.F., SLATER, S.A. & BATES, J.K. (1996): The release of uranium, plutonium, cesium, strontium, technetium and iodine from spent fuel under unsaturated conditions. *Radiochim. Acta* **74**, 65-71.

FRONDEL, C. (1958): Systematic mineralogy of uranium and thorium. *U.S. Geol. Surv., Bull.* **1064**.

HAWTHORNE, F.C. (1994) Structural aspects of oxides and oxysalt crystals. *Acta. Crystallogr.* **B50**, 481-510.

HAWTHORNE, F.C. (1997): Short-range order in amphiboles: a bond-valence approach. *Can. Mineral.* **35**, 201-216.

HIGGINS, S.R., EGGLESTON, C. M., KNAUSS, K.G. & BORO, C.O. (1998): A hydrothermal atomic force microscope for imaging in aqueous solutions up to 150°C. *Rev. Sci. Instrum.* **69**, 2994-2998.

HONESS, A.P. (1927): *The Nature, Origin and Interpretation of the Etch-Figures on Crystals*. John Wiley & Sons, New York, N.Y.

ISOBE, H., MURAKAMI, T. & EWING, R.C. (1992): Alteration of uranium minerals in the Koongarra deposit, Australia: unweathered zone. *J. Nucl. Mater.* **190**, 174-187.

JORDAN, G., HIGGINS, S. R., EGGLESTON, C.M., KNAUSS, K.G. & SCHMAHL, W.W. (2001): Dissolution kinetics of magnesite in acidic aqueous solution, a hydrothermal atomic force microscopy (HAFM) study: step orientation and kink dynamics. *Geochim. Cosmochim. Acta* **65**, 4257-4266.

KALINOWSKI, B.E. & SCHWEDA, P. (1996): Kinetics of muscovite, phlogopite and biotite dissolution and alteration at pH 1–4, room temperature. *Geochim. Cosmochim. Acta* **60**, 367-385.

LASAGA, A.C. (1983): Kinetics of silicate dissolution. *In* 4th Int. Symp. on Water–Rock Interaction (Misasa, Japan), 269-274.

LASAGA, A.C. & LÜTTGE, A. (2001): Variation of crystal dissolution rate based on a dissolution stepwave model. *Science* **291**, 2400-2404.

LI, YAPING & BURNS, P.C. (2000): Investigations of crystal-chemical variability in lead uranyl oxide hydrates. I. Curite. *Can. Mineral.* **38**, 727-735.

MEREITER, K. (1979): The crystal structure of curite, $[Pb_{6.56}(H_2O)OH)_4][(UO_2)_8O_8(OH)_6]_2$. *Tschermaks Mineral. Petrogr. Mitt.* **26**, 279-292.

RISTHAUS, P., BOSBACH, D., BECKER, U. & PUTNIS, A. (2001): Barite scale formation and dissolution at high ionic strength studied with atomic force microscopy. *Colloids Surf. A: Physicochemical and Engineering Aspects* **191/3**, 201-214.

RUFE, E. & HOCHELLA, M., JR. (1999): Quantitative assesment of reactive surface area of phlogopite dissolution during acid dissolution. *Science* **285**, 874-876.

SCHINDLER, M., MUTTER, A., HAWTHORNE, F.C. & PUTNIS, A. (2004a): Prediction of crystal morphology of complex uranyl-sheet minerals: theory. *Can. Mineral.* **42**, 1629-1650.

SCHINDLER, M., MUTTER, A., HAWTHORNE, F.C. & PUTNIS, A. (2004b): Prediction of crystal morphology of complex uranyl-sheet minerals: observation. *Can. Mineral.* **42**, 1651-1666.

SCHINDLER, M., HAWTHORNE, F.C., PUTNIS, C. & PUTNIS, A. (2004c): Growth of uranyl-hydroxy-hydrate and uranyl-carbonate minerals on the (104) calcite surface. *Can. Mineral.* **42**, 1683-1698.

SCHINDLER, M. & PUTNIS, A. (2004): AFM observations on the crystal growth of uranyl-oxide minerals on calcite. *Can. Mineral.* **42**, 1667-1682.

TAYLOR, J.C., STUART, W.L. & MUMME, I.A. (1981): The crystal structure of curite. *J. Inorg. Nucl. Chem.* **43**, 2419-2423.

TORRERO, M.E., CASAS, I., DE PABLO, J., SANDINO, M.C.A. & GRAMBOW, B. (1994): A comparison between unirradiated UO_2(s) and schoepite solubilities in 1 m NaCl medium. *Radiochim. Acta* **66/67**, 29-35.

WRONKIEWICZ, D.J., BATES, J.K., WOLF, S.F. & BUCK, E.C. (1996): Ten year results from unsaturated drip tests with UO_2 at 90°C: implications for the corrosion of spent nuclear fuel. *J. Nucl. Mater.* **238**, 78-95.

Received May 2, 2005, revised manuscript accepted September 9, 2005.